Quartile Based Differential Protection of Power Transformer

Ashesh M. Shah, Bhavesh R. Bhalja, *Senior Member, IEEE*, Rajesh M. Patel, Het Bhalja, Pramod Agarwal, *Member, IEEE*, Yogesh M. Makwana, *Member, IEEE*, and Om P. Malik, *Life Fellow, IEEE*

***Abstract*—A new technique for power transformer protection, that depends on the calculation of fault detection ratio (FDR) based on quartile of superimposed differential currents is presented. Internal faults are detected by comparing FDR with the predetermined threshold derived through analytical analysis and verified based on simulation results. The performance of the presented scheme is tested by modeling an existing Indian power transmission network using PSCAD/EMTDC software. Various types of abnormal conditions such as magnetizing inrush (including sympathetic and recovery) and over-excitation along with several types of internal (winding, inter-winding and turn-to-turn) faults have been investigated. Its validity has also been checked on the data of magnetizing inrush and simultaneous inrush with the internal fault in the transformer, which was obtained from the real network. The results reveal the effectiveness of the suggested technique in differentiating internal faults from other abnormal conditions. Further, it remains stable during heavy through fault with current transformer saturation. It is equally applicable for different ratings and winding connections of power transformers. Finally, comparative evaluation of the proposed scheme with the conventional and several existing techniques shows its superiority in terms of higher sensitivity during internal faults and improved stability in case of non-internal faults.**

***Index Terms*—Power transformer, differential protection, fault detection ratio and quartile of superimposed differential currents.**

I. Introduction

ALMOST 70–80% of faults that occur in power transformers are due to short-circuits in the winding and differential protection has been universally used as the primary protection [1], [2]. The conventional differential protection scheme is equipped with second harmonic restraint/bypass feature that offers discrimination between internal fault and non-internal fault events [3], [4]. Though the differential protection scheme accurately detects internal faults in the power transformer, it may face difficulty in correctly identifying non-internal faults like magnetizing inrush and over-excitation conditions. This is due to the decline of the second harmonic component in the transformer because of the utilization of low-loss core material. In addition, the percentage of second harmonic can also increase in the case of internal faults due to current transformer (CT) saturation phenomenon, which may create problems in the discrimination process.

In order to improve the sensitivity and reliability of the differential protection, approaches based on flux linkages and waveform identification have been proposed. Methods based on flux linkages [5], [6] issue a trip/block command depending on the change in windings flux linkages and deviation in generated voltages. However, the higher cost of accessories due to the requirement of different search coils makes the said schemes less attractive. Conversely, waveform identification based methods [7]–[10] identify internal faults by examining signatures of differential current and/or voltage based on fuzzy logic and artificial neural networks. Though the aforementioned methods yield good classification accuracy, the requirement of the large training dataset, excessive computation time, over-fitting of the data and tedious convergence rate may create difficulty in their implementation. Further, wavelet transform [11], [12] and mathematical morphology [13] based techniques have been introduced for differentiation between internal fault and non-internal faults. Nevertheless, wavelet based methods require a higher sampling rate and can be affected by noise and type of mother wavelet. In opposition, subjective prioritization of components and non-linearity due to the conditional ordering of morphology are a few limitations of the morphologically based method.

Later on, several researchers have explored schemes based on power differential waveform [14], [15] and the ratio of currents and voltages [16], [17]. However, the above methods involve voltage transformer besides the CT, which in turn increases the aggregate cost of the protection system. Subsequently, fault discrimination methods depending upon generalized delayed signal cancellation [18] and S-transform [19] have been presented. Nevertheless, instability due to nonlinearity in certain circumstances, implementation complexity, higher computational burden and redundant representation of the time-frequency

Manuscript received July 13, 2019; revised October 17, 2019 and December 11, 2019; accepted January 17, 2020. Date of publication January 22, 2020; date of current version September 23, 2020. This work was supported by Central Power Research Institute as a research program under Grant RSOP/2018/TR/03. Paper no.-TPWRD-00762-2019. *(Corresponding author: Bhavesh R. Bhalja.)*

A. M. Shah is with the Research scholar at Gujarat Technological University, Ahmedabad, Gujarat, India (e-mail: ashesh28@gmail.com).

B. R. Bhalja, H. Bhalja, and P. Agarwal are with the Department of Electrical Engineering, Indian Institute of Technology Roorkee, Roorkee, India (e-mail: bhaveshbhalja@gmail.com; hetbhalja18@gmail.com; pramgfee@iitr.ac.in).

R. M. Patel is with the Faculty of PG Studies and Research in Engineering and Technology, Marwadi Education Foundation Group of Institute's, Rajkot, Gujarat, India (e-mail: r_mpatel77@hotmail.com).

Y. M. Makwana is with the Department of Electrical Engineering, Government Engineering College, Dahod, Gujarat, India (e-mail: yogeshmakwana@gmail.com).

O. P. Malik is with the Department of Electrical and Computer Engineering, University of Calgary, Calgary, AB T2N 1N4, Canada (e-mail: maliko@ucalgary.ca).

Color versions of one or more of the figures in this article are available online at https://ieeexplore.ieee.org.

Digital Object Identifier 10.1109/TPWRD.2020.2968725

space can be the several shortcomings of the aforementioned techniques. Thereafter, methods based on empirical Fourier transform [20] and zone of non-saturation [21] have been presented. However, these schemes may not give acceptable results during over-excitation and sympathetic/recovery type of magnetizing inrush. Recently, a method based on fault related incremental currents using the positive and negative sequence components has been suggested [22]. However, the non-detection of three-phase fault, which is disastrous in nature, due to the absence of negative sequence component can be the prime limitation of the said scheme.

In order to overcome the said limitations, a new internal fault detection method based on quartile of superimposed differential currents is presented in this paper. The main benefit of the proposed method over several other existing methods is its ability to detect all types of internal faults such as Line-to-Ground (LG), Line-to-Line (LL), Line-to-Line-to-Ground (LLG), Line-to-Line-to-Line (LLL), Line-to-Line-to-Line-to-Ground (LLLG), inter-winding, and turn-to-turn. At the same time, unlike conventional methods, the suggested technique does not initiate a nuisance trip in case of non-internal faults. Moreover, it also provides correct operation in case of simultaneous inrush with the internal fault (energizing faulted power transformer event) during which most of the existing schemes may fail. Further, the suggested technique provides improved stability during heavy through fault with CT saturation condition. At the same time, it is applicable for different rating, winding topology, core geometry, winding resistance, leakage inductance and saturation inductance of the power transformer. Various test results obtained from diverse cases reveal that the proposed technique is robust and accurate against wide variation in fault and system parameters during internal faults, switching and saturation conditions in case of inrush as well as over-excitation, and CT saturation phenomenon. The proposed scheme provides comparable relay response time even with a low sampling frequency compared to other existing methods. In addition, evaluation using recorded field data of magnetizing inrush and internal fault for different power transformers clearly highlights the authenticity of the proposed method.

The proposed internal fault detection algorithm is described in Section II. Then, the simulation model and threshold selection are explained in Section III. The response of the suggested method for various cases is illustrated in Section IV. Comparative evaluation of the proposed method with conventional and recently developed techniques is discussed in Section V. Finally, Section VI concludes the paper.

II. Proposed Method

A. Basic Philosophy of Quartile

The selection of three quartiles (lower quartile (Q_1), median quartile (Q_2), and upper quartile (Q_3)) will distribute an orderly dataset (80 samples in this case) into four equal parts. Each part contains 25% (20 samples) of the total data (80 samples) [23]. The Q_2 distributes the data samples in two equal parts; half of the samples are above the median and the others are below the median. For the total '*m*' number of data samples containing dataset, $Y = \{Y_1, Y_2, \ldots Y_k, \ldots Y_m\}$ in which Y_k represents k^{th} sample of the dataset; $k = 1$ to m. This dataset is grouped in ascending order. Q_1 and Q_3 are obtained as the median of the first half and second half of the grouped dataset, respectively. The values of Q_1, Q_2 and Q_3 are calculated using (1) [23].

$$Q_{1/2/3} = Y_k + f \times (Y_{k+1} - Y_k) \tag{1}$$

where, k and f are the floor and fractional part of (m/4), (m/2) and (3m/4) for Q_1, Q_2 and Q_3, respectively. As the aforementioned three factors have been utilized in several applications [24]–[29], the same has been used in the proposed technique for discrimination between internal faults and non-internal faults in the power transformer.

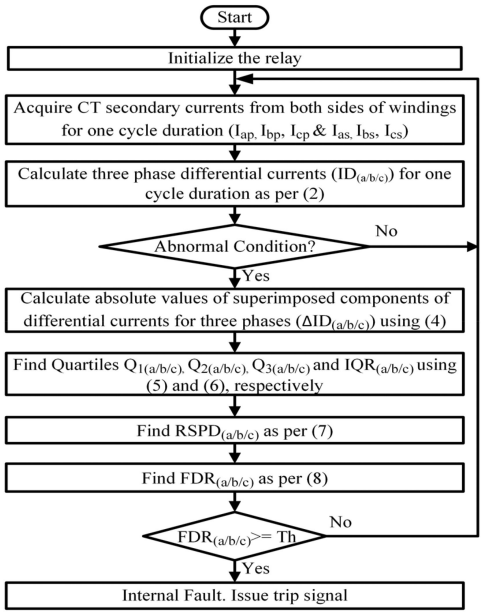

Fig. 1. Proposed algorithm.

B. Proposed Method

As shown in Fig. 1. instantaneous values of CT secondary currents are obtained from the primary (I_{ap}, I_{bp}, and I_{cp}) and secondary (I_{as}, I_{bs}, and I_{cs}) sides of the power transformer. After acquiring samples of CT secondary currents with a sampling frequency of 4 kHz (for a fundamental frequency of 50 Hz), instantaneous values of three-phase differential currents ($ID_{(a/b/c)}$) are calculated as per (2):

$$ID_{(a/b/c)} = \Big[MCF_p \times [CM] \times I_{(ap/bp/cp)} - MCF_s \times I_{(as/bs/cs)}\Big] \tag{2}$$

where, MCF_p and MCF_s are the magnitude compensation factor of the CT secondary current of primary and secondary windings of the transformer, respectively. The CM is the phase and zero sequence compensation matrix. For the proposed scheme, the

value of CM (for Yd1 connection) is given by (3).

$$\mathrm{CM} = \left(\frac{1}{\sqrt{3}}\right)\begin{bmatrix} 1 & 0 & -1 \\ -1 & 1 & 0 \\ 0 & -1 & 1 \end{bmatrix} \tag{3}$$

On the confirmation of an abnormal condition by abnormality detection algorithm [4], superimposed differential currents are calculated as per (4):

$$\Delta\mathrm{ID}_{(\mathrm{a/b/c})}(\mathrm{t}) = \mathrm{ID}_{(\mathrm{a/b/c})}(\mathrm{t}) - \mathrm{ID}_{(\mathrm{a/b/c})}(\mathrm{t}-\mathrm{T}) \tag{4}$$

where, $\Delta\mathrm{ID}_{(\mathrm{a/b/c})}$ (t) is the superimposed differential current for phases a, b, and c, respectively, at instant 't'. Further, 'T' is the window size (80 samples). Utilizing sliding window concept, absolute values of $\Delta\mathrm{ID}_{(\mathrm{a/b/c})}$ are used (after arranging in ascending order) to determine $\mathrm{Q}_{1(\mathrm{a/b/c})}$, $\mathrm{Q}_{2(\mathrm{a/b/c})}$ and $\mathrm{Q}_{3(\mathrm{a/b/c})}$ for each phase using (5) [23]–[26].

$$\mathrm{Q}_{\mathrm{P(a/b/c)}}(\mathrm{t}) = \Delta\mathrm{ID}_{(\mathrm{a/b/c})k} + f \times \left(\Delta\mathrm{ID}_{(\mathrm{a/b/c})\mathrm{k}+1} - \Delta\mathrm{ID}_{(\mathrm{a/b/c})\mathrm{k}}\right) \tag{5}$$

where, k and f are the floor and fractional part of (T/4), (T/2) and (3T/4) for P = 1, 2 and 3, respectively. Moreover, the value of the inter-quartile range (IQR), which is a measure of variability in the dataset, is calculated using (6).

$$\mathrm{IQR}_{(\mathrm{a/b/c})}(\mathrm{t}) = \mathrm{Q}_{3(\mathrm{a/b/c})}(\mathrm{t}) - \mathrm{Q}_{1(\mathrm{a/b/c})}(\mathrm{t}) \tag{6}$$

Then, these values are used to obtain a pre-detection index i.e., RSPD as per (7).

$$\mathrm{RSPD}_{(\mathrm{a/b/c})}(\mathrm{t}) = \left(\frac{\mathrm{Q}_{1(\mathrm{a/b/c})}(\mathrm{t})}{\mathrm{Q}_{3(\mathrm{a/b/c})}(\mathrm{t})}\right) \times \left(\mathrm{Q}_{2(\mathrm{a/b/c})}(\mathrm{t}) - \mathrm{Q}_{1(\mathrm{a/b/c})}(\mathrm{t})\right)^2 \tag{7}$$

Finally, fault detection ratio (FDR) is calculated as per (8), which is an indicator of internal fault in the transformer. This is achieved by phase wise comparison of the value of FDR with the pre-determined threshold. Here, the value of the threshold is selected as 4%. The procedure of threshold selection is thoroughly described in the next section. When the value of FDR exceeds threshold, an internal fault situation is identified which in turn initiates a trip signal. Conversely, in case when the said condition is not fulfilled, the trip signal is blocked due to the detection of a non-internal fault. With reference to (6), the value of FDR is considered as zero, when IQR = 0.

$$\mathrm{FDR}_{(\mathrm{a/b/c})}(\mathrm{t}) = \left(\frac{\mathrm{RSPD}_{(\mathrm{a/b/c})}(\mathrm{t})}{\mathrm{IQR}_{(\mathrm{a/b/c})}(\mathrm{t})}\right) \times 100\% \tag{8}$$

C. Validation of the Proposed Concept

The response of the proposed quartile based method in terms of graphical representation during internal fault and magnetizing inrush condition of the power transformer are shown in Figs. 2 to 5. The waveforms of differential current, superimposed differential current and quartiles in case of internal fault and magnetizing inrush condition are depicted in Fig. 2(a)–(c) and Fig. 3(a)–(c), respectively. The corresponding values of IQR, RSPD and FDR during an internal fault and magnetizing inrush condition are

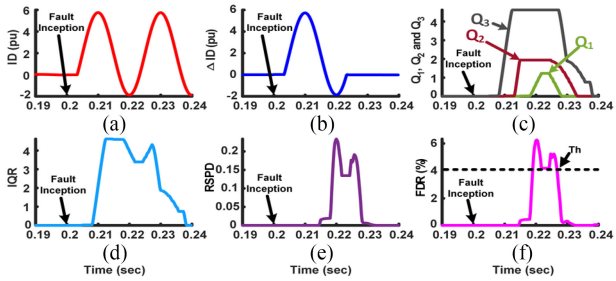

Fig. 2. Internal winding fault: (a) differential current, (b) superimposed current, (c) quartiles, (d) IQR, (e) RSPD and (f) FDR.

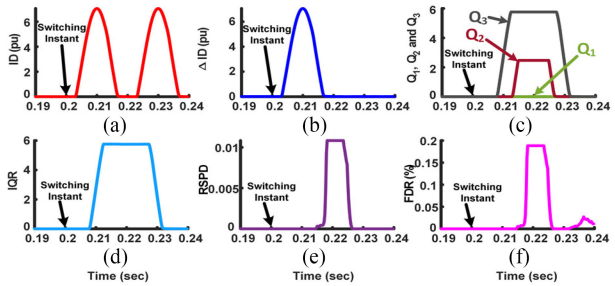

Fig. 3. Magnetizing inrush condition: (a) differential current, (b) superimposed current, (c) quartiles, (d) IQR, (e) RSPD and (f) FDR.

shown in Fig. 2(d)–(f) and Fig. 3(d)–(f), respectively. As observed from Fig. 2(c) and Fig. 3(c), a significant difference has been found in the value of Q_1 whereas marginal difference has been observed in the values of Q_2 and Q_3. Due to this fact, perceptible change has been noticed in the value of IQR (as it is obtained by subtracting the value of Q_1 from Q_3). Here, the IQR represents variation in the dataset. The major change of IQR depends on the magnitude of fault current as well as inrush. The waveform of IQR for internal fault and inrush condition not having a significant difference is shown in Fig. 2(d) and Fig. 3(d), respectively.

It has been observed from Fig. 2(d) and Fig. 3(d) that the value IQR is not able to discriminate between internal fault and magnetizing inrush situation. Hence, a new factor, known as RSPD that reflects a significant change in Q_1, Q_2 and Q_3, has been developed. The waveform of RSPD during internal fault and magnetizing inrush condition is shown in Fig. 2(e) and Fig. 3(e), respectively. Based on extensive simulations, it has been observed that the values of RSPD are almost equal during high magnitude of magnetizing inrush current and low magnitude of internal fault current. These two cases are depicted in Fig. 4 and Fig. 5. Subsequently, as observed from Fig. 4(d) and Fig. 5(d), the values of IQR are considerably dissimilar. Hence, a new factor known as FDR is developed for effective discrimination between the internal faults and magnetizing inrush conditions. The FDR is capable of providing proper discrimination as it has incorporated both IQR and RSPD. The waveforms of FDR during internal fault and magnetizing inrush condition are shown Fig. 2(f) and Fig. 3(f), respectively. It is observed from Figs. 2(f) and 4(f) that the value of FDR exceeds

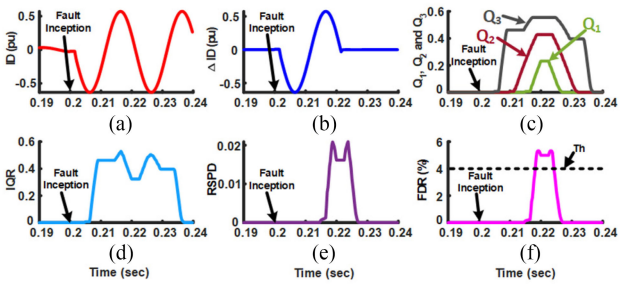

Fig. 4. Internal winding fault: (a) differential current, (b) superimposed current, (c) quartiles, (d) IQR, (e) RSPD and (f) FDR.

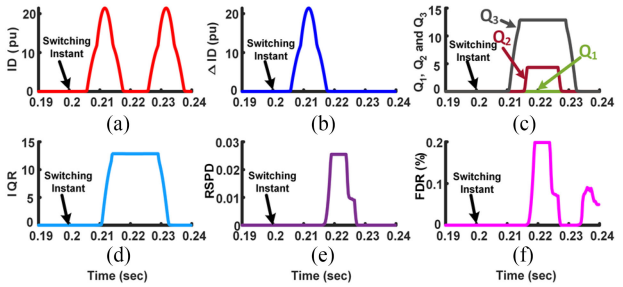

Fig. 5. Magnetizing Inrush condition: (a) differential current, (b) superimposed current, (c) quartiles, (d) IQR, (e) RSPD and (f) FDR.

threshold immediately after the inception of fault. Conversely, as observed from Figs. 3(f) and 5(f), the value of FDR stays well below the threshold during magnetizing inrush condition.

III. Simulation Model and Threshold Selection

A. Simulation Model

A single line diagram of a part of an existing Indian power transmission network, established and managed by Gujarat Electricity Transmission and Corporation (GETCO) limited, Gujarat, is shown in Fig. 6. The electrical power generated at 11 kV by public and private power producers is transmitted from generating station to the substation at 400 kV level, where it is stepped down to 220 kV level using power transformer. The simulation model, as shown in Fig. 6, developed in PSCAD/EMTDC software [30] for a 315 MVA, 400/220 kV, 50 Hz, Yd1 power transformer located at 400 kV Kasor substation, Gujarat, is capable of simulating internal faults, all types of inrush, over-excitation condition and CT saturation during external faults. Details of the power substation network, current transformer and power transformer are given in the Appendix.

B. Modelling of Turn-to-Turn and Inter-Winding Fault

As the tailor made inter-winding and turn-to-turn fault models are not available in PSCAD library, they have been developed as per [31]. The winding layout for modeling of transformer during normal condition, turn-to-turn and inter-winding faults is shown in Fig. 7(a), (b) and (c), respectively. For turn-to-turn and inter-winding faults, transformer is modeled using eight windings instead of six windings as shown in Fig. 7(b) and

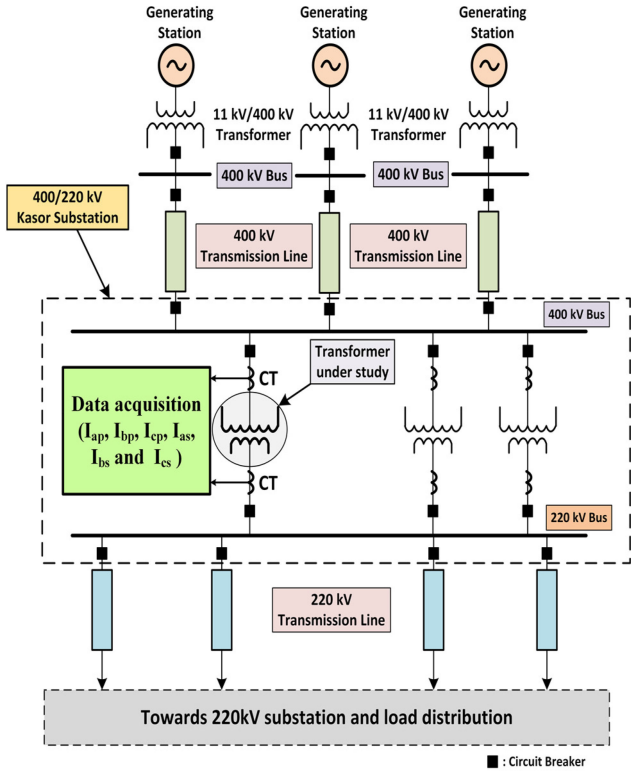

Fig. 6. Single line diagram of simulation model.

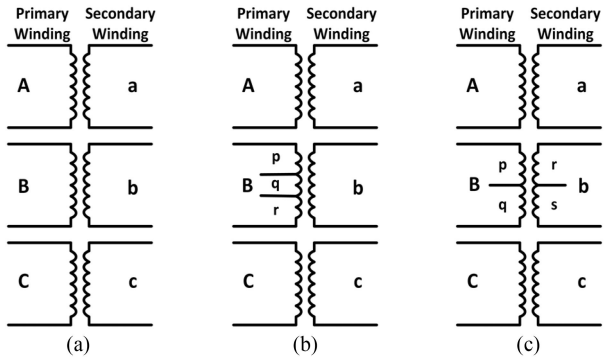

Fig. 7. Winding layout in case of (a) normal condition (b) turn-to-turn fault (c) inter-winding fault.

(c), respectively. Details of modelling for both faults are given below:

1) *Turn-to-turn fault:* In case of modelling of turn-to-turn fault, as depicted in Fig. 8(a), the winding involving turn-to-turn fault can be modelled as three separate windings i.e., p, q and r. With reference to Fig. 8, 'n_i' represents the total number of turns in i^{th} winding, where, i can be any individual winding (A, p, q, r, a, b, C and c). As shown in Fig. 8(a), during the pre-fault condition, all three windings i.e., p, q and r having turns ratio n_p, n_q and n_r, respectively, will work as a single winding 'B'. However, during the turn-to-turn fault, two windings (p and r) will be involved due to the shorting of 'q' winding. Here, n_p represents

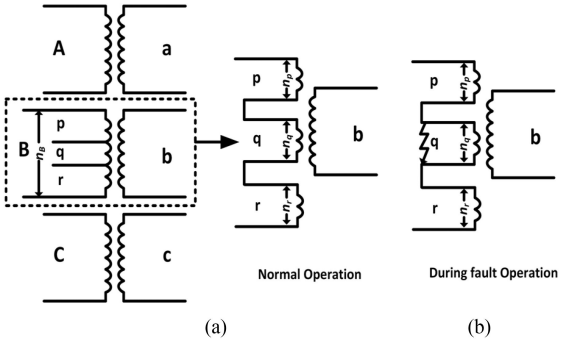

Fig. 8. Simulation layout of winding (for turn-to-turn) in case of (a) normal/Pre-fault condition (b) during fault condition.

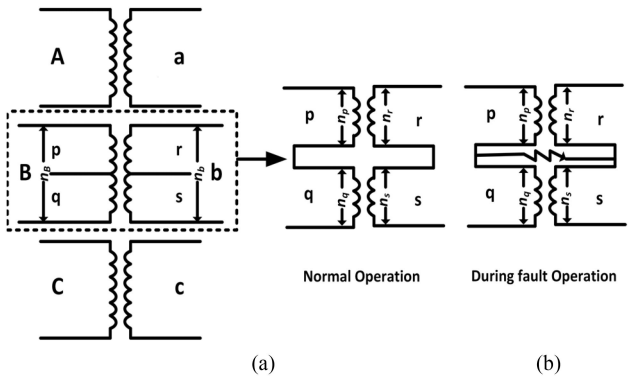

Fig. 9. Simulation layout of winding (inter-winding) in case of (a) normal/Pre-fault condition (b) during fault condition.

the number of turns at which the fault should be started (in percentage), n_q indicates the percentage of turns to be shorted and n_r indicates the percentage of remaining turns ($100\text{-}n_p\text{-}n_q$). The newly added elements of resistance matrix and inductance matrix of the transformer can be obtained using rules of consistency, leakage and proportionality.

2) *Inter-winding fault:* As depicted in Fig. 9(a), the windings involved in the inter-winding fault can be modelled as two separate windings i.e., p, q, r and s. With reference to Fig. 9, n_i represents the total number of turns in i^{th} winding, where, 'i' can be any individual winding (A, p, q, a, r, s, C and c). As shown in Fig. 9(a), during the pre-fault condition, all four windings i.e., p, q, r and s having turns ratio n_p, n_q, n_r and n_s, respectively, will work as a single winding 'B' and 'b'. During an inter-winding fault, four windings (p, q, r and s) will be involved as if 'B' and 'b' windings are shorted together. Here, n_p and n_r represent the number of turns at which the fault occurs. Similarly, n_q and n_s indicate the remaining turns. Due to the splitting of winding 'B' and 'b' into two sub-windings (p, q, r and s), the newly added elements of resistance matrix and inductance matrix of the transformer can be obtained using rules of consistency, leakage and proportionality.

TABLE I
GENERATED TEST CASES

Sr. No.	Operating condition	Parameters and their variation	Test cases
1	Winding faults	LG/LL/LLG/LLL/LLL/LLLG on each phase (11) × both sides of winding (2) × SI (3) × FL (5) × FIA (5)	1650
2	Inter-winding faults	Phases (3) × SI (3) × FL (5) × FIA (5)	225
3	Turn-to-turn faults	Phases (3) × both sides of winding (2) × SI (3) × percentage turn shorted (5) × FIA (5)	450
(I) Number of internal fault test cases generated			**2325**
4	Magnetizing inrush	Residual inrush (7) × SI (3) × SA (5) × load (5)	525
5	Sympathetic Inrush	SI (6) × SA (5) × load (5)	150
6	Recovery Inrush	Various external faults (8) × SI (3) × FIA (5)	120
7	Over-Excitation	Voltage (5) × Frequency (5) × SI (3) × SA (5)	375
(II) Number of test cases generated for non-internal faults			**1170**
Total numbers of test cases generated (I) + (II)			**3495**

C. Simulation of Test Cases

A large number of test cases, as depicted in Table I, have been generated on the developed simulation model of the transformer. Test cases for internal faults such as LG, LL, LLG, LLL, LLLG and inter-winding have been generated by varying fault location (FL) (5%, 25%, 50%, 75%, and 85% of the winding from the terminal) and fault inception angle (FIA) (0°, 30°, 60°, 90°, and 120° from the current zero of phase *'a'*) on both sides of the transformer. In the said cases, the system impedances (SIs), from the generating station to the power transformer, have also been varied (8 ∠85° Ω, 10 ∠85° Ω, and 12 ∠85° Ω). Moreover, test cases for turn-to-turn fault have been produced by simulating 0.3%, 0.5%, 1%, 3%, and 5% shorted turns on both sides of the windings of the transformer considering said variations.

Similarly, test cases for abnormal conditions like different magnetizing inrush and over-excitation conditions, as depicted in Table I, are also generated. Here, magnetizing inrush condition has been simulated by varying residual flux (0%, ±20%, ±50%, and ±80%), load (0%, 25%, 50%, 75%, and 100%), switching angle (SA) (0°, 30°, 60°, 90°, and 120° from the current zero of phase *'a'*) and above mentioned SI. Similarly, test cases for sympathetic inrush have been produced by considering aforementioned variation in SIs, SAs, and loads. Additionally, test cases for recovery inrush have been generated by varying external faults (LL, LLG, LLL and LLLG) and aforementioned SIs and FIAs. Likewise, the test cases for the over-excitation condition have been created by changing voltage level (110% to 120% of rated voltage in five equal steps) and frequency (48 to 50 Hz in five equal steps). It is to be noted from Table I that a total of 3495 simulation cases were generated out of which 2325 cases are for internal faults and 1170 cases are for non-internal faults.

D. Threshold Selection Based on Mathematical Calculation

The value of threshold, which plays a key role in the discrimination of internal fault from other non-internal faults, is derived

TABLE II
FDR VALUES OBTAINED USING ANALYTICAL STUDY

Sr. No.	Operating condition	Parameters and their variation range	Cases	Value of FDR (%)	
				Min	Max
1	Internal fault	FIA: 0° to 120° in steps of 15°, X: 0.1 to 0.3 in steps of 0.05, X_{th}/R_{th}: 10 to 30 in steps of 5.	9 × 5 × 5 = 225	7.21	61.19
2	Magnetizing inrush	SA: 0° to 120° in steps of 30°, θ_S: 0° to 90° in steps of 30°, X: 0.1 to 0.3 in steps of 0.05, X_{th}/R_{th}: 10 to 30 in steps of 5.	5 × 4 × 5 × 5 = 500	0	1.37
3	Over-excitation	V: 1.1 and 1.2 pu, θ_S: 30°, 40° and 50°, f: 49 and 50 Hz, X: 0.1 to 0.3 in steps of 0.05, X_{th}/R_{th}: 10 to 30 in steps of 5.	2 × 3 × 2 × 5 × 5 =300	0	0.08
		Total cases generated	1025		

by mathematical calculations. As per the analysis described in [32], [33], pre-fault, post-fault and magnetizing inrush current is given by (9), (10), and (11), respectively.

$$\mathrm{i(t)} = 0.949 \times \sin(\omega \mathrm{t} + \delta - 0.289) \tag{9}$$

$$\mathrm{i(t)} = 4.994 \times \begin{bmatrix} \sin(\omega \mathrm{t} + \delta - \gamma) \\ -0.9548 \times \exp(-18.85\mathrm{t}) \times \sin(\delta - \gamma - 0.189) \end{bmatrix} \tag{10}$$

$$\mathrm{i(t)} = \frac{1}{Z} \exp\left(\frac{-t}{\tau}\right) \begin{bmatrix} \sin(\omega t + \delta - \gamma_1) \\ -\exp\{-(\omega t + \theta_s) R_T/X\} \sin(\theta_s + \gamma_1) \end{bmatrix} \tag{11}$$

where, δ represents FIA in case of internal fault and SA during magnetizing inrush, $\gamma = \tan^{-1}(X_T/R_T)$ in which X_T and R_T are the transformer winding reactance and resistance, respectively. Further, Z is the impedance of the transformer after saturation, τ is the time constant for decay of residual flux, θ_S is the saturation angle of the transformer, $\gamma_1 = \tan^{-1}(X/R_T)$ in which X is the total reactance consisting of Thevenin's source reactance plus reactance of the transformer after saturation.

Similarly, as described in [34], the over-excitation condition can be represented by (12):

$$\begin{aligned} \mathrm{i(t)} &= \frac{V_m}{Z} \times (\cos(\omega t) - \cos(\theta_s)) \,; 0 \le \omega t \le \theta_s, 2\pi - \theta_s \\ &\le \omega t \le 2\pi \\ &= 0; \theta_s \le \omega t \le \pi - \theta_s; \pi + \theta_s \le \omega t \le 2\pi - \theta_s \\ &= \frac{V_m}{Z} \times (\cos(\omega t) + \cos(\theta_s)) \,; \pi - \theta_s \le \omega t \le \pi + \theta_s \end{aligned} \tag{12}$$

where, V_m is the maximum value of phase voltage.

In order to find an appropriate value of the threshold, variables given in (9)–(12) have been varied in a wide range (as shown in Table I) to produce current waveforms during internal fault (pre/post-fault), magnetizing inrush and over-excitation condition. As depicted in Table II, a total of 1025 cases of current waveforms and their FDRs have been generated. After performing analysis for internal faults, magnetizing inrush and over-excitation conditions, the maximum (Max) and the minimum (Min) values of FDR are depicted in Table II. It is to be noted from Table II that the Max and Min values of FDR for internal fault are 61.19% and 7.21%, respectively. Alternatively, the Min and the Max values of FDR for magnetizing inrush and over-excitation condition are found to be 0% and 1.37% and 0% and 0.08%, respectively.

TABLE III
FDR VALUES OBTAINED THROUGH SIMULATION STUDY

Operating Condition	Value of FDR (%)		Operating Condition	Value of FDR (%)	
	Min	Max		Min	Max
Internal fault conditions			Non-internal faults		
Winding faults	5.26	80.19	Magnetizing inrush	0	2.48
Inter-winding faults	28.40	65.68	Sympathetic inrush	0	2.09
Turn-to-turn faults	4.64	69.87	Recovery inrush	0	0.08
			Over-excitation	0	0.12

E. Threshold Validation Based on Simulation Results

In order to validate the threshold value of FDR analytically, various simulation cases, as mentioned in Table I, have been evaluated. After acquiring samples of CT secondary currents from both sides of the transformer for each of the simulation cases, the value of FDR is derived as per (8). The obtained Min and Max values of FDR during various internal faults and non-internal faults are depicted in Table III.

It is observed from Table III that the Min value of FDR is 4.64% during turn-to-turn fault whereas its Max value is 2.48% in case of non-internal fault cases (all types of inrush and over-excitation). Though the threshold value from analytical derivation does not match with the simulation study, the only purpose of the said verification is to determine the maximum generalized value of threshold (so that nuisance trip can be avoided). Here, the threshold value is decided by incorporating safety margin in the base value of threshold (maximum of either analytical or simulation study). In the proposed scheme, the maximum value of FDR comes out to be 2.48% from the simulation study. Hence, considering approximately 150% of the safety margin, 4% value of threshold has been decided. This value is generalized in nature and can be applicable even in case of different ratings, winding topology, core geometry, winding resistance, leakage inductance and saturation inductance of the power transformer.

IV. PERFORMANCE EVALUATION

Responses for the selected cases in terms of FDR are discussed in this section.

A. Winding Faults

Waveforms of the differential currents and FDR for all phases, during a LG fault at 95% of winding from the terminal with 0°FIA on the HV side, are shown in Fig. 10(a) and (b), respectively. It is noted from Fig. 10(b) that the value of FDR for phases

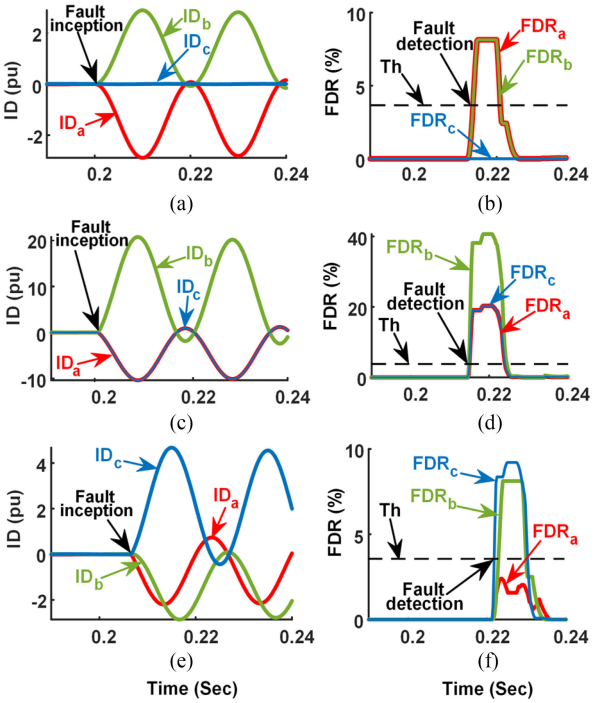

Fig. 10. Differential currents (a), (c) and (e) and FDRs (b), (d) and (f) during LG fault, LL fault, and LLG fault.

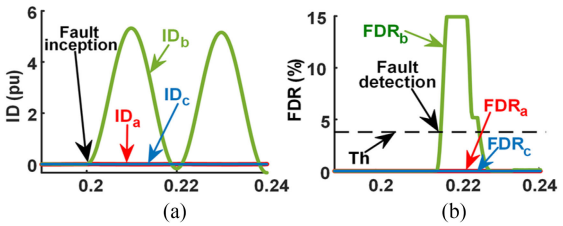

Fig. 11. Inter-winding fault (a) differential currents (b) FDRs.

'a' and *'b'* increases from 0% to around 8% within a cycle after the inception of fault at 0.2 s. Likewise, Fig. 10(c) and (d) show similar waveforms during a LL fault between phases *'a'* and *'b'* at 80% of winding from the terminal with 0°FIA on HV side of the power transformer. It is observed from Fig. 10(d) that the value of FDR increases from 0% to 20%, 40% and 20% for phases *'a'*, *'b'*, and *'c'*, respectively. Likewise, refering to Fig. 10(f), during a LLG fault for phases *'b'* and *'c'* at 95% winding from terminal on the HV side at 120°FIA, the FDR reaches to maximum of 2.5%, 9%, and 10% for phases *'a'*, *'b'*, and *'c'*, respectively. It is observed from the aforementioned three fault cases that the proposed algorithm detects an internal fault condition when the value of FDR crosses the threshold for any of the three phases.

B. Inter-Winding and Turn-to-Turn Faults

The waveforms of differential currents and FDRs for inter-winding fault at 50% of winding with SI = 12 $\angle$ 85° Ω and fault impedance = 0.1 Ω on phase *'b'* are depicted in Fig. 11(a) and (b), respectively. As observed from Fig. 11(b), the value of FDR exceeds the threshold and hence, the proposed scheme initiates a trip signal. Subsequently, Fig. 12(a) to (c) show the waveforms of differential current, superimposed differential current and quartiles for a turn-to-turn fault with 0.3% shorted turns at 0° FIA on phase 'a' of HV winding of the transformer. Furthermore, the values of IQR, RSPD and FDR are depicted in Fig. 12(d), (e) and (f), respectively. It is to be noted from Fig. 12(d)–(f) that the values of IQR, RSPD and FDR are quite comparable to that of the low level of internal fault case (refer Fig. 4(d)–(f)). In this case, as observed from Fig. 12(f), the proposed scheme is able to detect low level turn-to-turn fault up to 0.3% shorted turns involving fault impedance of the order of 0.01 Ω as the value of FDR exceeds the threshold. This is because of the low value of IQR, which comes in the denominator in the equation of FDR even though the value of RSPD (which comes in the numerator) remains almost equal during both cases i.e., low-level turn-to-turn fault and internal fault cases. It is to be noted that the proposed scheme may fail to detect the turn-to-turn fault occurring below 1% shorted turns with a high value of fault impedance. However, the probability of occurrence of low level turn-to-turn faults with a high value of impedance is very rare [35], [36].

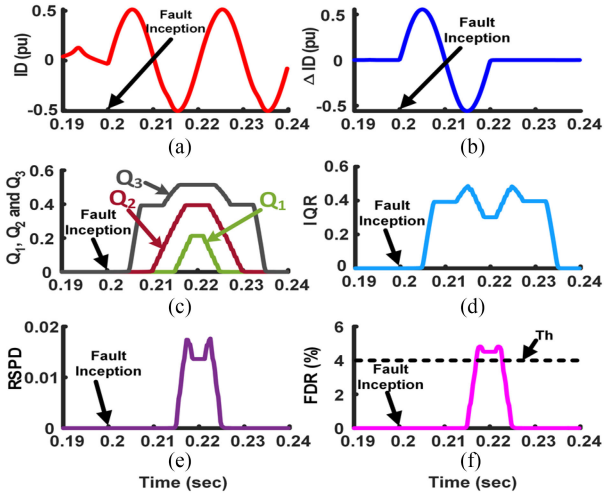

Fig. 12. Turn-to-turn fault (a) differential current, (b) superimposed differential current, (c) quartiles, (d) IQR, (e) RSPD and (f) FDR.

C. Magnetizing Inrush and Over-Excitation

The waveform of differential currents and FDRs during transformer energization at no load with 0° SA are shown in Fig. 13(a) and (b), respectively. It is observed from Fig. 13(b) that the values of FDR stay well below the threshold. Furthermore, a recovery inrush occurs when an external fault is eliminated and the voltage has regained the normal value. This situation is created by performing an external LLG fault at 0°FIA and the waveforms of differential currents and FDRs are shown in Fig. 13(c) and (d), respectively. As observed in Fig. 13(d), the maximum value of FDR remains well below the threshold. Moreover, Fig. 13(e) and (f) show the waveforms of differential currents and FDRs, respectively, during sympathetic inrush at no

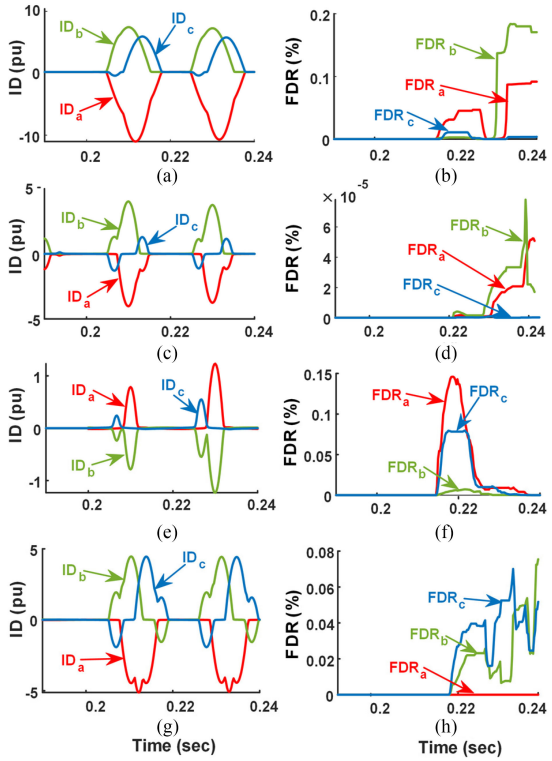

Fig. 13. Differential currents (a), (c), (e) and (g) and FDRs (b), (d), (f) and (h) during magnetizing inrush, recovery inrush, sympathetic inrush and over-excitation.

load with 0° SA. It can be seen from Fig. 13(f) that the maximum value of FDR remains near 0.15%, which is much lower than the threshold. Therefore, the proposed algorithm remains stable for all types of magnetizing inrush conditions and does not initiate the nuisance trip. In case of the over-excitation condition, the biased differential relay may mal-operate and detect the situation as an internal fault. To show the effectiveness of the proposed technique against the over-excitation condition, a test case for the rise in terminal voltage to 120% of rated voltage and reduction in fundamental frequency to 48 Hz has been simulated. The obtained waveforms of differential currents and FDRs are shown in Fig. 13(g) and (h), respectively. It is observed from Fig. 13(h) that the values FDR for all phases remain significantly lower than the threshold.

D. Effect of CT Saturation During Internal and External Faults

It is widely acknowledged that the imprecise current magnitude due to CT saturation during external fault may lead to mal-operation of the conventional differential relay. The robustness of the proposed scheme during severe CT saturation condition has been evaluated during external as well as an internal fault. For an external fault, an external LL fault (phases 'b' and 'c') on the adjacent transmission line at 10 km with 0°FIA with high CT burden resistance has been simulated. Figs. 14(a) and (b) show the waveforms of CT secondary currents and FDRs, respectively, in the said situation. As observed in Fig. 14(b),

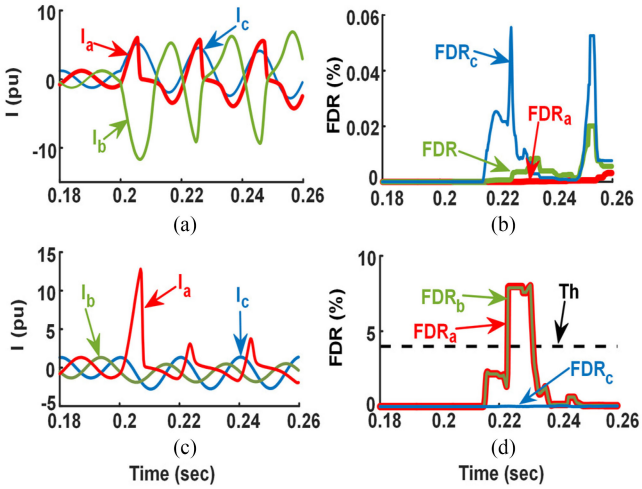

Fig. 14. (a) and (c) CT secondary currents (b) and (d) FDRs during an external and an internal fault with CT saturation, respectively.

the maximum value of FDR stays well below the threshold, which in turn blocks the operation of the relay. Conversely, an internal LG fault on phase 'a' at 85% of winding location from its terminal on the HV side with 0°FIA with severe CT saturation has been simulated. The waveforms of CT secondary currents and FDRs are depicted in Fig. 14(c) and (d), respectively. It is observed from Fig. 14(d) that the value of FDR exceeds the threshold and hence, confirms an internal fault situation.

E. Performance Evaluation on Data Collected From Field

Investigation of the relay on the data recorded from the real sub-station, which signifies effectively in-zone fault and inrush situation experienced by the power transformer, plays a vital role in ensuring a correct equilibrium among security and dependability. The GETCO, Gujarat, India has recorded real data of currents during the energization of a faulted 5 MVA, 33/11 kV, 50 Hz Yd11 transformer. It has also recorded data of currents in case of a magnetizing inrush situation during energization of a 1500 MVA, 765/400 kV, 50 Hz, Dy11 transformer. For both the aforementioned cases, the signature is captured by the fault recorder of the relay at a sampling frequency of 1 kHz with a fundamental frequency of 50 Hz. These waveforms, further extracted from the COMTRADE file of the relay, are utilized for verifying the performance of the proposed scheme.

The non-linearity and momentary events are included now in real time fault data and hence, the suggested technique is assessed in the real-world situations [37]. The response of the proposed technique has been evaluated for two sample cases. Waveforms of differential current and FDR for all phases while energizing a faulted transformer during an internal fault on phase *'b'* are shown in Fig. 15(a) and (b), respectively. It is observed from Fig. 15(b) that the computed values of FDR surpass the threshold and hence, the trip command is issued by the relay. Moreover, the waveforms of differential current and FDR during magnetizing inrush conditions at no-load are shown in Fig. 15(c) and (d), respectively. It is noted from Fig. 15(d)

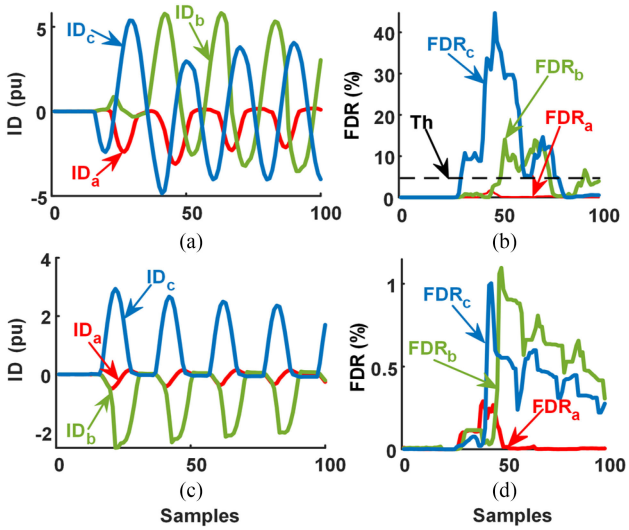

Fig. 15. (a) Differential currents and (b) FDRs during energization of a faulted transformer (c) differential currents and (d) FDRs during magnetizing inrush.

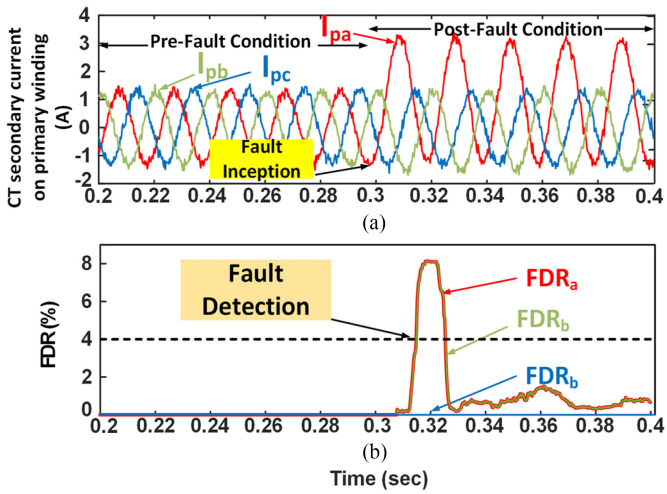

Fig. 16. (a) CT secondary currents containing noise (20 dB) (b) FDRs.

that the maximum value of FDR for all phases remains well below the threshold. The above discussion clearly indicates that the proposed technique is capable to differentiate between an internal fault and the magnetizing inrush condition.

F. Effect of Noise

All digital/numerical relays consist of a signal conditioning block, which contains isolation transformer, surge protection circuit and Anti-Aliasing Filter (AAF) [34]. However, the performance of the proposed scheme has been evaluated during a L-G fault at 95% of phase '*a*' on HV winding of the transformer along with the presence of noise. The instantaneous values of CT secondary currents of all three phases (I_{pa}, I_{pb} and I_{pc}) on HV winding of the transformer with SNR = 20 dB are shown in Fig. 16(a). It is mentioned in the literature that the typical value of SNR is larger than 27 dB for power system signal analysis [38].

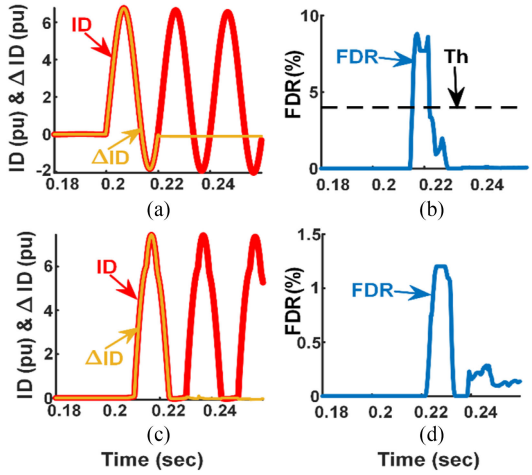

Fig. 17. (a) and (c) Differential and superimposed currents (b) and (d) FDR during an internal fault and magnetizing inrush condition, respectively.

Hence, to evaluate the performance of the suggested scheme in a worse situation, the value of SNR is chosen as 20 dB. As observed from the response of the proposed scheme, Fig. 16(b), the value of FDR stays almost zero before the inception of fault. However, after the occurrence of a fault, the value of FDR exceeds the pre-defined threshold. Hence, the proposed algorithm detects the situation as a fault even when the noise is present in the acquired signal.

G. Response During Different Rating and Winding Connection

In this regard, a simulation on 160 MVA, 132 kV/ 220 kV, Yd11, 50 Hz transformer, located at Kasor substation, Gujarat, is carried out. The outcome of the proposed scheme in terms of differential current, superimposed differential current and the value of FDR during an internal LG fault and magnetizing inrush condition is shown in Fig. 17(a) and (b) and Fig. 17(c) and (d), respectively. As observed in Fig. 17(b), the value of FDR exceeds the threshold during an internal fault whereas it remains well below the threshold in case of magnetizing inrush condition (refer Fig. 17(d)). Hence, the suggested method equally works on different rating and winding connections of the power transformer and provides satisfactory results.

V. Comparative Assessment of the Proposed Scheme

Comparative assessment of the proposed technique with several existing techniques based on conventional biased differential protection scheme [39], non-saturation (NSZ) [21], correlation coefficient (CC) [40], second central moment (SCM) [41], Wavelet transform (WT) [12], magnetizing hysteresis (MH) [42], Chirplet transform (ChT) [43] and generalized delayed signal cancelation (GDSC) [18] is described in Table IV. It is observed from Table IV that all the aforementioned methods may fail to sense inter-winding faults whereas the proposed technique detects them efficiently. Furthermore, most of the said techniques may initiate a nuisance trip in case of the over-excitation condition and they require a greater number of

TABLE IV
COMPARATIVE ASSESSMENT OF THE PROPOSED SCHEME

Operating Condition		Conventional [39]	NSZ [21]	CC [40]	SCM [41]	WT [12]	MH [42]	ChT [43]	GDSC [18]	Proposed Method
Winding faults	Asymmetrical	√	√	√	√	√	√	√	√	√
	Symmetrical	√	√	×	×	√	×	√	×	√
Inter-winding faults		×	×	×	×	×	×	×	×	√
Turn-to-turn faults		×	√	√	√	√	√	√	×	√
Magnetizing inrush		√	√	√	√	√	√	√	√	√
Over-excitation		√	×	×	×	×	√	×	×	√
CT saturation during heavy through fault		√	√	√	√	√	√	√	√	√
Energization of faulted transformer		×	√	×	√	√	√	√	×	√
Average operating time in case of internal faults (ms)		20	20	2.5	< 20	< 1	20	15	5-20	15-20
Sampling Frequency (kHz)		4	7.8	10	30.72	15.36	20	1.6	15.36	4
√ and × indicates operating condition considered and not considered, respectively.										

samples per cycle. In addition, unlike several existing methods, as depicted in Table IV, the proposed method is also capable of detecting symmetrical winding faults such as LLL and LLLG.

Moreover, the average relay operation time of the proposed technique is almost comparable with other methods. Though the method based on GDSC and Wavelet claimed very low response time, they require high sampling frequency. Further, the technique based on GDSC may wrongly classify the event because of the introduction of error in the estimation of phase sequence component particularly during major grid disturbances [44], whereas the Wavelet-based method is susceptible to noise.

The sampling frequency of the proposed method is lower than the other methods, which yields low power consumption, reduced cost, smooth data capturing for Analog-to-Digital Converter (ADC) and easier interface with Field Programmable Gate Array (FPGA). Subsequently, though ChT based method has low sampling rate, it requires high computation time due to the complexity involved in the algorithm.

VI. CONCLUSION

A new FDR based method, derived from quartiles of superimposed differential currents, for the protection of power transformer is presented. It is demonstrated that the derived FDR is capable of distinguishing all types of internal faults from magnetizing inrush and over-excitation conditions with the exception of turn-to-turn fault in the presence of the inrush current. The suggested technique detects winding and inter-winding faults including turn-to-turn faults within one power frequency cycle. It is not vulnerable to the influence of CT saturation in the case of external as well as internal fault conditions. It remains secure for all types of magnetizing inrush and over-excitation situations including noise present in the acquired signals. At the same time, it is equally applicable on different rating and winding connection of power transformer. Moreover, verification of its performance on actual field data (containing energization of faulted transformer and magnetizing inrush condition) reveals its correctness in detecting internal faults and immunity against nuisance trip during non-internal faults. Finally, comparative assessment of the proposed technique in terms of coverage of different types of internal fault, stability during external disturbances, average relay operation time and sampling frequency requirement demonstrates its benefits in comparison with other existing methods.

APPENDIX

Source Impedance	Z_1	0.8715 + j9.9615 Ω
	Z_0	1.743 + j19.923 Ω
Power Transformer	Rating	3-phase, 315 MVA, 400 kV/220 kV, 50 Hz
	Connection	YΔ1
	Reactance (per phase)	12.5%
	Magnetizing Current	0.1%
Current Transformer	Ratio	1/433
	Leakage Inductance	0.8 mH
	Burden Resistance	0.5 Ω

REFERENCES

[1] J. L. Blackburn and T. J. Domin, *Protective Relaying: Principles and Applications*, 3rd ed. New York, NY, USA: Taylor & Francis Group, 2007.

[2] IEEE Guide for Protecting Power Transformers. IEEE Standard C37. 91-2008 (Revision of IEEE Std. C37.91-2000). I. S. Jacobs and C. P. Bean, "Fine particles, thin films and exchange anisotropy," in *Magnetism*, vol. III, G. T. Rado and H. Suhl, Eds. New York: Academic, 1963, pp. 271–350.

[3] R. Hamilton, "Analysis of transformer inrush current and comparison of harmonic restraint methods in transformer protection," *IEEE Trans. Ind. Appl.*, vol. 49, no. 4, pp. 1890–1899, Jul. 2013.

[4] A. Ashrafian, B. Vahidi, and M. Mirsalim, "Time–time-transform application to fault diagnosis of power transformers," *IET Gener. Transmiss. Distrib.*, vol. 8, no. 6, pp. 1156–1167, Jun. 2014.

[5] Y. C. Kang, B. E. Lee, S. H. Kang, and P. A. Crossley, "Transformer protection based on the increment of flux linkages," *IEEE Proc. Gener. Transmiss. Distrib.*, vol. 151, no. 4, p. 548, Jul. 2004.

[6] F. Haghjoo, M. Mostafaei, and H. Mohammadi, "A new leakage flux-based technique for turn-to-turn fault protection and faulty region identification in transformers," *IEEE Trans. Power Del.*, vol. 33, no. 2, pp. 671–679, Apr. 2018.

[7] D. Barbosa, U. C. Netto, D. V. Coury, and M. Oleskovicz, "Power transformer differential protection based on Clarke's transform and fuzzy systems," *IEEE Trans. Power Del.*, vol. 26, no. 2, pp. 1212–1220, Apr. 2011.

[8] R. Naresh, V. Sharma, and M. Vashisth, "An integrated neural fuzzy approach for fault diagnosis of transformers," *IEEE Trans. Power Del.*, vol. 23, no. 4, pp. 2017–2024, Oct. 2008.

[9] M. R. Zaman and M. A. Rahman, "Experimental testing of the artificial neural network based protection of power transformers," *IEEE Trans. Power Del.*, vol. 13, no. 2, pp. 510–517, Apr. 1998.

[10] D. V. Coury and E. C. Segatto, "An alternative approach using artificial neural networks for power transformer protection," *Eur. Trans. Elect. Power*, vol. 16, no. 1, pp. 63–77, 2006.
[11] R. P. Medeiros, F. B. Costa, and K. M. Silva, "Power transformer differential protection using the boundary discrete wavelet transform," *IEEE Trans. Power Del.*, vol. 31, no. 5, pp. 2083–2095, Oct. 2016.
[12] R. P. Medeiros and F. B. Costa, "A wavelet-based transformer differential protection with differential current transformer saturation and cross-country fault detection," *IEEE Trans. Power Del.*, vol. 33, no. 2, pp. 789–799, Apr. 2018.
[13] Q. Wu, T. Ji, M. Li, and W. Wu, "Using mathematical morphology to discriminate between internal fault and inrush current of transformers," *IET Gener. Transmiss. Distrib.*, vol. 10, no. 1, pp. 73–80, Jan. 2016.
[14] K. Yabe, "Power differential method for discrimination between fault and magnetizing inrush current in transformers," *IEEE Trans. Power Del.*, vol. 12, no. 3, pp. 1109–1118, Jul. 1997.
[15] A. Hooshyar, S. Afsharnia, M. Sanaye-Pasand, and B. M. Ebrahimi, "A new algorithm to identify magnetizing inrush conditions based on instantaneous frequency of differential power signal," *IEEE Trans. Power Del.*, vol. 25, no. 4, pp. 2223–2233, Oct. 2010.
[16] E. Ali, A. Helal, H. Desouki, K. Shebl, S. Abdelkader, and O. P. Malik, "Power transformer differential protection using current and voltage ratios," *Elect. Power Syst. Res.*, vol. 154, pp. 140–150, Jan. 2018.
[17] E. Ali, O. P. Malik, S. Abdelkader, A. Helal, and H. Desouki, "Experimental results of ratios-based transformer differential protection scheme," *Int. Trans. Elect. Energy Syst.*, vol. 29, no. 11, pp. 1–14, Jul. 2019.
[18] Y. N. Batista, H. E. P. de Souza, F. de A. dos Santos Neves, and R. F. D. Filho, "A GDSC-based technique to distinguish transformer magnetizing from fault currents," *IEEE Trans. Power Del.*, vol. 33, no. 2, pp. 589–599, Apr. 2018.
[19] S. R. Samantaray, B. K. Panigrahi, P. K. Dash, and G. Panda, "Power transformer protection using S-transform with complex window and pattern recognition approach," *IET Gener. Transmiss. Distrib.*, vol. 1, no. 2, pp. 278–286, 2007.
[20] S. Kumar Murugan, S. P. Simon, K. Sundareswaran, P. S. R. Nayak, and N. P. Padhy, "An empirical Fourier transform-based power transformer differential protection," *IEEE Trans. Power Del.*, vol. 32, no. 1, pp. 209–218, Feb. 2017.
[21] A. Sahebi and H. Samet, "Efficient method for discrimination between inrush current and internal faults in power transformers based on the nonsaturation zone," *IET Gener. Transmiss. Distrib.*, vol. 11, no. 6, pp. 1486–1493, Apr. 2017.
[22] N. Farzin, M. Vakilian, and E. Hajipour, "Transformer turn-to-turn fault protection based on fault-related incremental currents," *IEEE Trans. Power Del.*, vol. 34, no. 2, pp. 700–709, Apr. 2019.
[23] G. Upton and I. Cook, *Understanding Statistics*. USA: Oxford University Press, 1997.
[24] S. Taran and V. Bajaj, "Rhythm-based identification of alcohol EEG signals," *IET Sci. Meas. Technol.*, vol. 12, no. 3, pp. 343–349, May 2018.
[25] X. Shen, X. Fu, and C. Zhou, "A combined algorithm for cleaning abnormal data of wind turbine power curve based on change point grouping algorithm and quartile algorithm," *IEEE Trans. Sustain. Energy*, vol. 10, no. 1, pp. 46–54, Jan. 2019.
[26] Y. Zhao, L. Ye, W. Wang, H. Sun, Y. Ju, and Y. Tang, "Data-driven correction approach to refine power curve of wind farm under wind curtailment," *IEEE Trans. Sustain. Energy*, vol. 9, no. 1, pp. 95–105, Jan. 2018.
[27] T. T. Pham, C. Thamrin, P. D. Robinson, A. L. McEwan, and P. H. W. Leong, "Respiratory artefact removal in forced oscillation measurements: A machine learning approach," *IEEE Trans. Biomed. Eng.*, vol. 64, no. 8, pp. 1679–1687, Aug. 2017.
[28] M. A. Motin, C. K. Karmakar, and M. Palaniswami, "ensemble empirical mode decomposition with principal component analysis: A novel approach for extracting respiratory rate and heart rate from photoplethysmographic signal," *IEEE J. Biomed. Heal. Informat.*, vol. 22, no. 3, pp. 766–774, May 2018.
[29] H.-C. Shih and E.-R. Liu, "Automatic reference color selection for adaptive mathematical morphology and application in image segmentation," *IEEE Trans. Image Process.*, vol. 25, no. 10, pp. 4665–4676, Oct. 2016.
[30] Manitoba HVDC Research Centre, User's guide on the use of PSCADTM - Power Systems Computer Aided Design v4.6(2018), 2005. [Online]. Available: https://hvdc.ca/uploads/knowledge_base/pscad_manual_v4_6.pdf?t=1528395602, Accessed on: Jun. 20, 2019.
[31] P. Bastard, P. Bertrand, and M. Meunier, "A transformer model for winding fault studies," *IEEE Trans. Power Deliv.*, vol. 9, no. 2, pp. 690–699, Apr. 1994.
[32] M. A. Rahman, P. K. Dash, and E. R. Downton, "Digital protection of power transformer based on weighted least square algorithm," *IEEE Trans. Power App. Syst.*, vol. PAS-101, no. 11, pp. 4204–4210, Nov. 1982.
[33] H. K. Verma and G. C. Kakoti, "Algorithm for harmonic restraint differential relaying based on the discrete Hartley transform," *Elect. Power Syst. Res.*, vol. 18, no. 2, pp. 125–129, 1990.
[34] S. H. Horowitz and A. G. Phadke, *Power System Relaying*, 3rd ed. New York: John Wiley & Sons Ltd, 2008.
[35] Satish V. Kulkarni and S. A. Khaparde, *Transformer engineering: design, technology, and diagnostics*. Boca Raton, FL, USA: CRC Press, 2017.
[36] "IEEE guide for protecting power transformers," in IEEE Std C37.91-2008 (Revision of IEEE Std C37.91-2000), vol., no., pp. 1–139, May 30, 2008.
[37] M. Sanaye-Pasand and O. P. Malik, "High speed transmission line directional protection evaluation using field data," *IEEE Trans. Power Del.*, vol. 14, no. 3, pp. 851–856, Jul. 1999.
[38] M. Pazoki, "A new fault classifier in transmission lines using intrinsic time decomposition," *IEEE Trans. Ind. Informatics*, vol. 14, no. 2, pp. 619–628, Feb. 2018.
[39] ABB, Application manual on Transformer protection RET670, version 2.2 ANSI, 2019. [Online]. Available: https://search-ext.abb.com/library/Download.aspx?DocumentID=1MRK504163-UUS&LanguageCode=en&DocumentPartId=&Action=Launch, Accessed on: Jul. 9, 2019.
[40] A. A. A. Etumi and F. J. Anayi, "The application of correlation technique in detecting internal and external faults in three-phase transformer and saturation of current transformer," *IEEE Trans. Power Del.*, vol. 31, no. 5, pp. 2131–2139, Oct. 2016.
[41] H. Esponda, E. Vazquez, M. A. Andrade, and B. K. Johnson, "A setting-free differential protection for power transformers based on second central moment," *IEEE Trans. Power Del.*, vol. 34, no. 2, pp. 750–759, Apr. 2019.
[42] Z. Jiao and Z. Li, "Novel magnetization hysteresis-based power-transformer protection algorithm," *IEEE Trans. Power Del.*, vol. 33, no. 5, pp. 2562–2570, Oct. 2018.
[43] S. Kumar Murugan, S. P. Simon, P. S. R. Nayak, K. Sundareswaran, and N. P. Padhy, "Power transformer protection using chirplet transform," *IET Gener. Transmiss. Distrib.*, vol. 10, no. 10, pp. 2520–2530, 2016.
[44] M. Bongiorno, J. Svensson, and A. Sannino, "Effect of sampling frequency and harmonics on delay-based phase-sequence estimation method," *IEEE Trans. Power Del.*, vol. 23, no. 3, pp. 1664–72, Jul. 2008.

Ashesh M. Shah received the B.E. degree in electrical engineering from Birla Vishvakarma Mahavidyalaya Engineering College, Sardar Patel University, Anand, India, in 1999 and the M.E. degree in electrical engineering from The Maharaja Sayajirao University of Baroda, Vadodara, India, in 2002. He is currently working toward the Ph.D. degree in electrical engineering with Gujarat Technological University, Ahmedabad, India. He is currently an Assistant Professor with the Department of Electrical Engineering, Government Engineering College, Bharuch, India.

Bhavesh R. Bhalja (Senior Member, IEEE) received the B.E. and M.E. degrees in electrical engineering from Birla Vishvakarma Mahavidyalaya Engineering College, Sardar Patel University, Anand, India, in 1999 and 2001, respectively, and the Ph.D. degree from the Indian Institute of Technology (IIT) Roorkee, Roorkee, India, in 2007. He has a teaching experience of more than 19 years. He is currently an Associate Professor with the Department of Electrical Engineering, IIT Roorkee. He has Authored and Coauthored more than 100 papers in referred international journals. His research interests include digital protection and automation, smart grid technologies and applications, distributed generation, micro-grid, power quality improvement, and application of artificial intelligence. He is the recipient of Fulbright-Nehru Academic and Professional Excellence Fellowships, Young Engineers Award, Merit Award, and Pandit Madan Mohan Malviya Award by Institution of Engineers, India.

Rajesh M. Patel received the B.E. degree in electrical engineering from Government Engineering College, Modasa, India, in 1998, the M.E. degree in electrical engineering from Lalbhai Dalpatbhai College of Engineering, Ahmedabad, India, in 2000, and the Ph.D. degree from the Indian Institute of Technology Roorkee, Roorkee, India, in 2011. He is currently a Professor and Head of the Electrical Engineering Department, Faculty of Engineering, Marwadi Education Foundation Group of Institutions, Rajkot, India. His research interests include condition monitoring, power system protection, vibration analysis, and artificial intelligence.

Het Bhalja received the B.Tech. and M.Tech. degrees in electrical engineering from Pandit Deendayal Petroleum University, Gandhinagar, India, in 2017 and 2019, respectively. He is currently working toward the Ph.D. degree with the Department of Electrical Engineering, Indian Institute of Technology Roorkee, Roorkee, India. His research interests include digital protection, electrical machines, substation automation, multi-level inverters, reneable emergy generation, microgrid and electric vehicles.

Pramod Agarwal (Member, IEEE) received the B.E., M.E., and Ph.D. degrees in electrical engineering from the Indian Institute of Technology Roorkee, Roorkee, India, in 1983, 1985, and 1995, respectively. Since 2004, he has been a Professor with the Department of Electrical Engineering, Indian Institute of Technology Roorkee. His current research interests include power electronics, smart grids, multilevel inverters, power quality improvement, and application of power electronics in power system.

Yogesh M. Makwana (Member, IEEE) received the B.E. degree in electrical engineering from North Gujarat University, Patan, India, in 2002, the M.E. degree in electrical engineering from Maharaja Sayajirao University of Baroda, Vadodara, India, in 2004, and the Ph.D. degree from the Indian Institute of Technology Roorkee, Roorkee, India, in 2018. He is currently an Assistant Professor with the Department of Electrical Engineering, Government Engineering College, Dahod, India. His research interests include digital protection of power system, smart grids technologies and applications, distributed generation, and micro-grids protection.

Om P. Malik (Life Fellow, IEEE) received the bachelor's degree in 1952, the M.E. degree in electrical machine design from the University of Roorkee, Roorkee, India, in 1962, the Ph.D. degree in electrical engineering from the University of London, London, U.K., in 1965, and the D.I.C. degree from the Imperial College of Science and Technology, London. In 1968, he joined the University of Calgary, Calgary, AB, Canada, where he is currently a Professor Emeritus with the Department of Electrical and Computer Engineering. He is a Fellow of the Engineering Institute of Canada, of the Canadian Academy of Engineering, and of the Institution of Electrical Engineers. He is also actively involved in IFAC and is currently a Chair of the IFAC Technical Committee on Power Plants and Power Systems Control.